JACS
JOURNAL OF THE AMERICAN CHEMICAL SOCIETY
Article
pubs.acs.org/JACS

Influence of Donor–Acceptor Distance Variation on Photoinduced Electron and Proton Transfer in Rhenium(I)–Phenol Dyads

Martin Kuss-Petermann, Hilke Wolf, Dietmar Stalke, and Oliver S. Wenger*

Institut für Anorganische Chemie, Georg-August-Universität Göttingen, Tammannstrasse 4, D-37077 Göttingen, Germany

Supporting Information

ABSTRACT: A homologous series of four molecules in which a phenol unit is linked covalently to a rhenium(I) tricarbonyl diimine photooxidant via a variable number of *p*-xylene spacers (n = 0–3) was synthesized and investigated. The species with a single *p*-xylene spacer was structurally characterized to get some benchmark distances. Photoexcitation of the metal complex in the shortest dyad (n = 0) triggers release of the phenolic proton to the acetonitrile/water solvent mixture; a H/D kinetic isotope effect (KIE) of 2.0 ± 0.4 is associated with this process. Thus, the shortest dyad basically acts like a photoacid. The next two longer dyads (n = 1, 2) exhibit intramolecular photoinduced phenol-to-rhenium electron transfer in the rate-determining excited-state deactivation step, and there is no significant KIE in this case. For the dyad with n = 1, transient absorption spectroscopy provided evidence for release of the phenolic proton to the solvent upon oxidation of the phenol by intramolecular photoinduced electron transfer. Subsequent thermal charge recombination is associated with a H/D KIE of 3.6 ± 0.4 and therefore is likely to involve proton motion in the rate-determining reaction step. Thus, some of the longer dyads (n = 1, 2) exhibit photoinduced proton-coupled electron transfer (PCET), albeit in a stepwise (electron transfer followed by proton transfer) rather than concerted manner. Our study demonstrates that electronically strongly coupled donor–acceptor systems may exhibit significantly different photoinduced PCET chemistry than electronically weakly coupled donor–bridge–acceptor molecules.

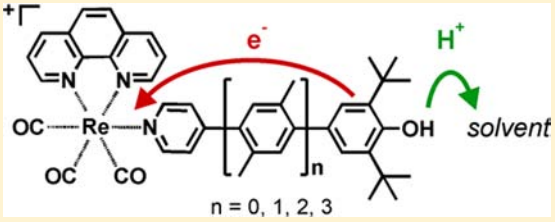

INTRODUCTION

Proton-coupled electron transfer (PCET) is an important elementary step in many biochemical processes, photosynthesis being a particularly relevant example.[1−8] If we are to emulate natural photosynthesis in artificial systems, a thorough understanding of all factors governing PCET rates and efficiencies appears indispensable. Although fundamental aspects of PCET chemistry can be investigated directly on suitable enzymes, the use of chemically simpler artificial molecular models is very popular.[9] Phenols are attractive in this context because their hydroxylic proton becomes highly acidic upon oxidation,[10,11] allowing these molecules to act as combined electron/proton donors.[12−14] Certain phenol systems can be viewed as models for the Tyr_Z/His-190 PCET interface in photosystem II (Scheme 1a):[13,15−29] light absorption by chlorophyll leads to the formation of a highly oxidizing porphyrin molecule ($P_{680}^{\bullet+}$) that is reduced by Tyr_Z, and presumably this is coupled to transfer of the phenolic proton to the nearby His-190 base.[6,30] A central question of many fundamental PCET investigations is whether the overall reaction is a concerted process or proceeds by individual electron- and proton-transfer steps. Many phenol-containing systems react via concerted proton–electron transfer (CPET),[13,15−29] but stepwise mechanisms in which initial electron transfer is followed by proton transfer (ETPT) have also been reported.[31−33] Some aspects regarding the PCET chemistry of phenols have received particular attention in recent years, such as the influence of solvent pH on driving forces and rates, the importance of buffer ions as proton acceptors, and the special role played by water as a medium in which PCET takes place.[34−39]

Scheme 1. (a) PCET between the Tyrosine$_Z$, Histidine$_{190}$, and Chlorophyll P_{680} Components of Photosystem II; (b) Rhenium(I) Tricarbonyl Photosensitizers with Appended 2,6-Di-*tert*-butylphenol Units Investigated in This Work (n = 0–3)

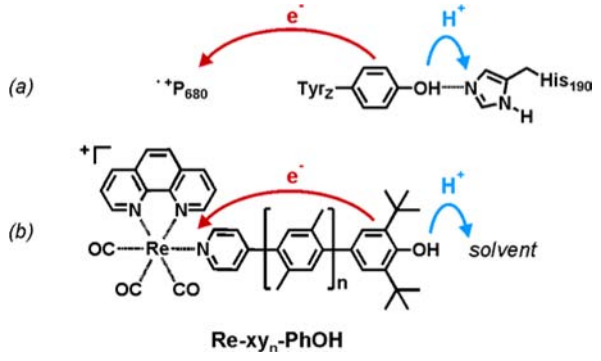

It is not uncommon for the participating electron to be transferred over a significantly longer distance than the proton

Received: June 1, 2012
Published: July 18, 2012

   dx.doi.org/10.1021/ja3053046 | J. Am. Chem. Soc. 2012, 134, 12844–12854

during the course of a PCET reaction. There are systems in which the CPET mechanism is dominant even though electron donor and electron acceptor are separated by more than 6 Å. However, while the distance dependence of pure electron transfer has long been studied,[40,41] the distance dependence of PCET is yet poorly explored and has only recently come into the focus of attention.[42−45] PCET has in fact four relevant distances, namely, the electron- and proton-transfer distances and the separations between the proton and the electron in the donor and the acceptor. Here we focus on the influence of the distance between the proton- and electron-accepting units in bidirectional (multisite) PCET with the rigid rodlike molecules shown in Scheme 1b. 2,6-Di-*tert*-butylphenol (PhOH) serves as a combined electron−proton donor, a tricarbonyl(phenanthroline)(pyridine)rhenium(I) complex (Re) is the photooxidant, and a solvent molecule in the immediate neighborhood of the phenol acts as the proton acceptor. The distance between the two redox partners was varied from 7.9 to 20.8 Å through the introduction of one, two, or three *p*-xylene (xy) units, leading to a simultaneous increase in the distance between the electron-accepting center and the proton-accepting site. These molecules can be viewed as functional models for the Tyr_Z/His-190/P_{680} reaction triple of photosystem II.

RESULTS AND DISCUSSION

Synthesis and X-ray Crystal Structure. The synthesis of the molecules from Scheme 1b was performed in a modular fashion as described previously by us for analogous rhenium/ruthenium−(oligo-*p*-xylene)−phenothiazine systems.[46−50] Detailed synthetic protocols and molecule characterization data are given in the Supporting Information. The result of an X-ray crystal structure analysis of Re−xy_1−PhOH is shown in Figure 1.

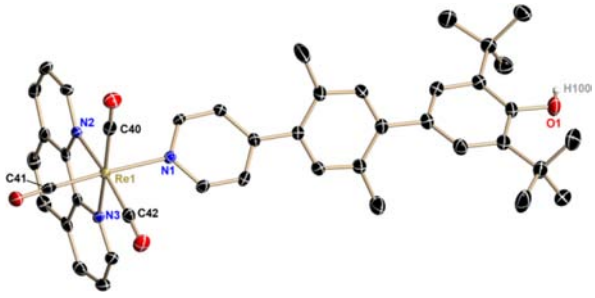

Figure 1. Crystallographic structure of the Re−xy_1−PhOH cation. Anisotropic displacement parameters are drawn at the 50% probability level. Hydrogen atoms, anions, and cocrystallized solvent molecules have been omitted.

Re−xy_1−PhOH crystallizes in the monoclinic space group *C*2/*c* with a single molecule in the asymmetric unit containing the Re−xy_1−PhOH unit and the triflate counterion. Additionally, a dichloromethane and a disordered diethyl ether solvent molecule are present in the asymmetric unit. As shown in Figure 1, the Re atom is coordinated by three carbonyl, one pyridine, and one phenanthroline ligand to form an almost perfect octahedral coordination polyhedron. While the equatorial positions are occupied by two carbonyls and the phenanthroline ligands, the perfect square is only slightly distorted, with the N3−Re−N2 angle being the smallest at 75.94° and the N2−Re−C40 angle being the largest at 97.26° (Table 1). At one of the axial positions is a carbonyl group, while the other vertex is formed by the pyridine−xy_1−PhOH entity. The C41−Re−N1 unit forms an almost perfectly linear arrangement, with an angle of 177.72°. Regarding the Re−N bonds, one finds the axial Re−N bond to be slightly elongated compared with the equatorial ones (2.205 Å vs 2.175/2.181 Å, respectively). Thus, the bond lengths vary within the expected range. The three Re−CO bonds are almost all of the same length, showing no elongation in the axial position.

Table 1. Selected Bond Lengths and Angles

bond	bond length (Å)	angle unit	bond angle (deg)
Re1−N1	2.205(2)	N2−Re1−N3	75.94(9)
Re1−N2	2.181(3)	C42−Re1−C40	91.86(14)
Re1−N3	2.175(3)	N2−Re1−C40	97.26(12)
Re1−C40	1.920(4)	N3−Re1−C42	94.98(12)
Re1−C41	1.928(3)	C41−Re1−N1	92.25(11)
Re1−C42	1.912(3)		

The most important piece of information that can be extracted from this structure is that the distance between the center of the phenol and the rhenium atom is 12.2 Å, corresponding to the center-to-center electron-transfer distance in this compound. One further extracts a length of 4.3 Å for a xylene repeating unit, and we thus conclude that the electron donor−acceptor distances (R_{DA}) in Re−xy_0−PhOH, Re−xy_2−PhOH, and Re−xy_3−PhOH are 7.9, 16.5, and 20.8 Å, respectively. In the structure of Re−xy_1−PhOH, the dihedral angle between the phenol and xylene planes (57°) and that between the xylene and pyridine planes (41°) are in the typical range for oligo-*p*-phenylene systems.[51−54] However, while the magnitude of these torsion angles has an important influence on the electronic coupling between the donor and acceptor,[55−57] little can be learned from the solid-state structure regarding the situation in solution.

Optical Absorption and Emission. Figure 2a shows the UV−vis spectra of the four molecules from Scheme 1b (solid lines) in acetonitrile solution. The purple dashed line is the spectrum of the trifluoromethanesulfonate salt of $[Re(phen)(CO)_3(py)]^+$ (phen = 1,10-phenanthroline; py = pyridine), which was used as a reference complex (hereafter called "Re-ref") incapable of exhibiting any PCET, proton transfer, or intramolecular electron transfer reactivity. All five absorption spectra show a prominent absorption maximum at 275 nm due to a phenanthroline-localized $\pi-\pi^*$ transition.[58,59] In the spectrum of Re−xy_0−PhOH there is a band maximum at 323 nm due to a transition with phenol-to-pyridine charge transfer (CT) character.[60] The intensity of this band decreases rapidly with increasing donor−acceptor distance, already being noticeable merely as a shoulder in the spectrum of Re−xy_1−PhOH. This is an important observation because it demonstrates how rapidly the electronic communication between PhOH and Re decreases as a function of distance; on the other hand, this observation is not much of a surprise, given the known exponential distance dependence of superexchange interactions and the fact that a *p*-xylene spacer has a length of ∼4.3 Å.[41,61,62]

Bridge lengthening was further observed to lead to increasing extinction at wavelengths shorter than 350 nm, which can be explained by increasing π conjugation between mutually connected phenol, *p*-xylene, and pyridine units. As is commonly the case for rhenium(I) tricarbonyl diimines, metal-to-ligand charge transfer (MLCT) absorptions occur at ∼380 nm.[58]

dx.doi.org/10.1021/ja3053046 | J. Am. Chem. Soc. 2012, 134, 12844−12854

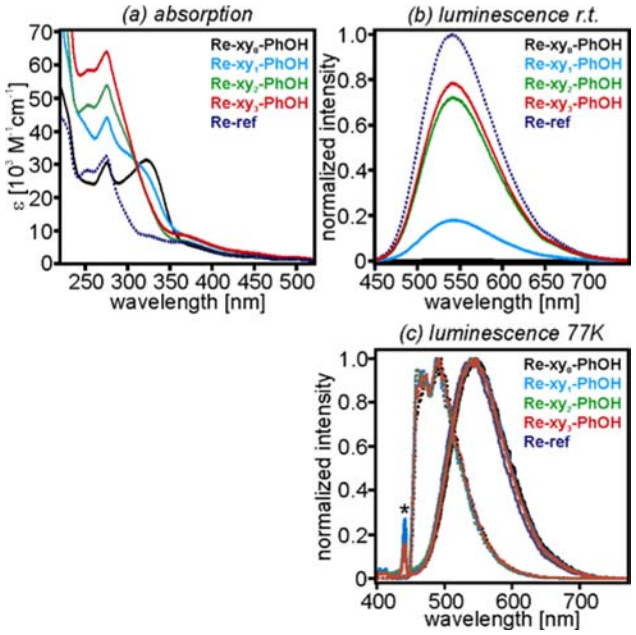

Figure 2. (a) Optical absorption spectra of the four molecules from Scheme 1b and a reference complex in acetonitrile solution. (b) Normalized luminescence spectra of the same compounds in 1:1 (v/v) acetonitrile/water at 25 °C. Excitation occurred at 410 nm. It should be noted that the emission spectrum of Re−xy_0−PhOH almost coincides with the *x* axis. (c) Normalized luminescence spectra of the same compounds in MTHF at room temperature (solid lines) and at 77 K (dashed lines). Excitation occurred at 410 nm. The asterisk in (c) denotes Raman scattering peaks.

Figure 2b shows that the lowest-lying ^{3}MLCT states are emissive in all five compounds in 1:1 (v/v) acetonitrile/water solution, albeit with significantly different luminescence quantum yields. Following excitation at 410 nm with corrections for differences in absorbance between individual solutions at this wavelength, the strongest emission was observed for the reference complex, while the luminescence of the Re−xy_n−PhOH molecules became weaker with decreasing donor−acceptor distance (decreasing *n*). For *n* = 0, the emission spectrum almost coincided with the *x* axis. We note that in the protic CH_3CN/H_2O mixture considered here, the luminescence lifetime of Re−xy_0−PhOH is much shorter than that of Re-ref (40 vs 1270 ns; see below), so the intensity and lifetime decreases go hand in hand when CH_3CN is mixed with H_2O. The observation of increasing luminescence quenching with decreasing *n* signals the presence of a nonradiative excited-state deactivation process that is dependent on the phenol−rhenium distance. Emission quenching by triplet−triplet energy transfer can be ruled out on thermodynamic grounds: the $[Re(phen)(CO)_3(py)]^+$ complex has a triplet energy (E_T) of ~2.75 eV,[63] while (unsubstituted) phenol has E_T = 3.55 eV[64] and the *p*-xylene units can be expected to have even higher triplet energies.[65] Consequently, the emission quenching observed in Figure 2b is most likely due to either photoinduced electron transfer, proton transfer, or a combination of the two (PCET).

Given the observation of strong rhenium(I)−phenol coupling in Re−xy_0−PhOH, we performed low-temperature emission experiments in order to test whether the emissive excited state is indeed the same in all four dyads. Figure 2c shows the results from experiments in which 10^{-5} M solutions of the dyads in 2-methyltetrahydrofuran (MTHF) were excited at 390 nm at room temperature (solid lines) and at 77 K as frozen solutions (dashed lines). The four emission spectra were normalized arbitrarily to an intensity of 1.0 at the emission band maximum for better direct comparison. This procedure made it obvious that the four emission bands are virtually identical, and one may conclude that the emissive excited state is the same in all four dyads, at least at 77 K. However, the relative energies of excited states of rhenium(I) tricarbonyl diimines can change in going from fluid solutions to rigid glasses,[58] so we cannot know for sure whether at 298 K the conclusion from above still holds true. On the other hand, there was no evidence for a rigidochromic effect in our systems. The observation of vibrational fine structure in 77 K emission spectra is common for rhenium(I) tricarbonyl diimines and signals the participation of intraligand ($\pi-\pi^*$) states in the low-temperature luminescence.[58,59]

Cyclic Voltammetry. The electrochemical potentials of the redox-active phenol and rhenium(I) units in the four dyads from Scheme 1b were determined using cyclic voltammetry. The actual voltammograms are shown in the Supporting Information; here we merely report the redox potentials as determined in dry acetonitrile solution in the presence of 0.1 M tetrabutylammonium hexafluorophosphate ($TBAPF_6$) as the electrolyte (Table 2).

The first thing we note is that the phenol oxidations are irreversible, as frequently observed for phenols.[10] In this situation, we estimated the half-wave potential from the inflection point occurring in the rise of the respective redox wave when sweeping from low to high potential. There appeared to be no dependence of the redox potentials determined in this manner on the potential sweep rate, at least not in the range between 10 and 300 mV/s.

Table 2. Center-to-Center Electron Donor−Acceptor Distances (R_{DA}), Electrochemical Potentials, and Driving Forces for Photoinduced Electron Transfer (ΔG_{ET}) in the Four Dyads from Scheme 1b

		electrochemical potentials (V vs Fc^+/Fc)[a]			
dyad	R_{DA} (Å)	$E(PhOH/PhOH^+)$	$E(PhO^-/PhO^\bullet)$	$E(Re^I/Re^0)$	ΔG_{ET} (eV)
Re−xy_0−PhOH	7.9	1.20	−0.28	−1.57	+0.00
Re−xy_1−PhOH	12.2	1.01	−0.59	−1.54	−0.20
Re−xy_2−PhOH	16.5	0.98	−0.64	−1.54	−0.22
Re−xy_3−PhOH	20.9	0.99	−0.63	−1.54	−0.21

[a] $E(PhOH/PhOH^+)$ is the electrochemical potential for oxidation of the phenol component in the dyads, $E(PhO^-/PhO^\bullet)$ is the potential for oxidation of the deprotonated form of the phenol, and $E(Re^I/Re^0)$ is the electrochemical potential for reduction of the rhenium(I) unit in the four dyads. The electrochemical potentials were measured in dry acetonitrile solution containing 0.1 M $TBAPF_6$. See the Supporting Information for the voltammograms.

dx.doi.org/10.1021/ja3053046 | J. Am. Chem. Soc. 2012, 134, 12844−12854

The shortest member (Re−xy$_0$−PhOH) stands out from the dyad series in that it exhibits a phenol oxidation potential that is markedly different from those of the three longer congeners (Re−xy$_{1-3}$−PhOH). Oxidation of the 2,6-di-*tert*-butylphenol unit in Re−xy$_0$−PhOH occurs at a potential of 1.2 V vs Fc^+/Fc, while in the Re−xy$_{1-3}$−PhOH dyads, potentials of only ∼1.0 V vs Fc^+/Fc are necessary (Figure S1 in the Supporting Information). This is yet another manifestation of the stronger interaction of the phenol with its neighboring molecular units in Re−xy$_0$−PhOH compared with the longer dyads (in addition to the observation of phenol-to-pyridine CT absorption bands in Re−xy$_0$−PhOH,[60] as described above). We initially presumed that because of the proximity of the cationic rhenium(I) complex, the phenol unit in Re−xy$_0$−PhOH is oxidized less readily than in the longer congeners, where the electrostatic influence from the metal site is expected to be weaker. However, cyclic voltammetry of the free pyridine−xy$_n$−PhOH ligands (Figure S3 in the Supporting Information) revealed that this is not primarily an electrostatic effect, as the observed difference of ∼0.2 V between the phenol oxidation potentials of the free ligands was similar to that between Re−xy$_0$−PhOH and Re−xy$_{1-3}$−PhOH. It appears plausible that the true physical origin of this 0.2 V potential shift is a strong electronic interaction between phenol and pyridine when these two units are coupled directly to one another. The reason for this may be the electron-withdrawing character of pyridine.

Upon deprotonation of the phenol units by the addition of sodium methoxide, the resulting phenolate moieties are oxidized at −0.28 V vs Fc^+/Fc in Re−xy$_0$−PhO$^-$ and at about −0.6 V vs Fc^+/Fc in Re−xy$_{1-3}$−PhO$^-$, again showing a substantial difference between the shortest member and the longer members of the series (Table 2, fourth column). An analogous observation was made for the free ligands (Figure S4 in the Supporting Information). For the shortest deprotonated ligand, one may draw two resonance structures (Scheme 2),

Scheme 2. Two Resonance Structures of the Phenolate−Pyridine Ligand in Deprotonated Re−xy$_0$−PhOH

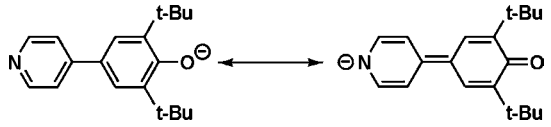

which may help provide an understanding of why this molecular unit is oxidized less readily than the *p*-xylene-bridged congeners: negative charge can simply be delocalized toward the metal center. We note that this interpretation is in line with the assignment of the 323 nm absorption band in the UV−vis spectrum of Re−xy$_0$−PhOH (Figure 1a) to a phenol-to-pyridine CT transition (see above).[60]

Addition of sodium methoxide to solutions of rhenium(I) tricarbonyl diimine complexes is of some concern because the presence of coordinating CH_3O^- may lead to ligand substitution reactions, particularly at the axial position where the pyridine is located.[66] However, on the basis of the observation of clear differences between the cyclic voltammograms of the shortest member of the series and the longer congeners not only for the dyads but also for the corresponding free ligands (Figures S2 and S4, respectively, in the Supporting Information), we conclude that substitution of the pyridine ligand did not occur to an extent significant for electrochemical investigations.

In the Re−xy$_{0-3}$−PhOH dyads, the Re moiety is reduced at potentials between −1.54 and −1.57 V vs Fc^+/Fc (Table 2, fifth column), in line with literature values for reduction of rhenium(I) tricarbonyl diimines.[58]

On the basis of the phenol oxidation potentials (E_{ox}) and rhenium(I) reduction potentials (E_{red}) from Table 1, one can use eq 1 to estimate ΔG_{ET}, the driving force for photoinduced electron transfer from the phenol to the ^{3}MLCT-excited rhenium complex:[67]

$$\Delta G_{ET} = e(E_{ox} - E_{red}) - E_{00} + \frac{e^2}{4\pi\varepsilon_0 r}\left(\frac{1}{\varepsilon_s} - \frac{1}{\varepsilon_{ref}}\right) \quad (1)$$

In eq 1, E_{00} is the energy of the photoactive ^{3}MLCT state of the rhenium complex (2.75 eV),[63] ε_0 is the vacuum permittivity, r is the average radius of the two involved redox partners (assumed to be 4.5 Å), ε_s the dielectric constant of the solvent in which the electrochemical potentials were determined (for acetonitrile, ε_s = 35.94), and ε_r is the dielectric constant of the solvent used for the spectroscopic measurements [for 1:1 (v/v) acetonitrile/water, ε_r = 55.7].[68] This analysis leads to the conclusion that electron transfer from the phenol unit to the photoexcited rhenium(I) moiety is expected to be slightly exergonic in the Re−xy$_{1-3}$−PhOH dyads (Table 2, last column) but should have essentially no driving force in Re−xy$_0$−PhOH. We note that driving force estimates based on eq 1 are accurate to 0.1 eV at best, particularly in view of the fact that some of the redox waves are irreversible (see above).

Phenol Deprotonation. The pK_a value of the phenol in Re−xy$_0$−PhOH in 1:1 (v/v) CH_3CN/H_2O was determined via UV−vis titration, monitoring the absorption change at 431 nm upon addition of aqueous sodium hydroxide solution (Figure 3a). The midpoint of the titration was found to occur at a pH

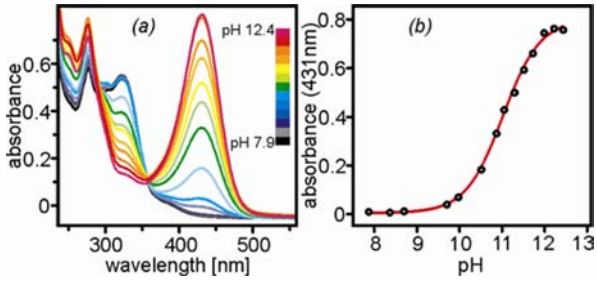

Figure 3. (a) Absorption spectra of Re−xy$_0$−PhOH in 1:1 (v/v) acetonitrile/water at different pH values. (b) Titration curve obtained by monitoring the absorbance change at 431 nm.

meter reading of 11.0 (Figure 3b), corresponding to an effective pK_a value of 11.3 in 1:1 (v/v) acetonitrile/water.[69] Substantially less prominent spectral changes were observed upon deprotonation of the longer congeners because the phenol−pyridine coupling is weaker in Re−xy$_{1-3}$−PhOH than in Re−xy$_0$−PhOH (titration data not shown). For the Re−xy$_2$−PhOH dyad, we found a pK_a value of 11.4 [effective pK_a in 1:1 (v/v) CH_3CN/H_2O]. Acetonitrile/water mixtures had to be used for these experiments because the triflate salts of our complexes are insoluble in pure water and because the acetonitrile/water mixture was also employed for (time-resolved) luminescence and transient absorption spectroscopy (see below).

Time-Resolved Emission. Table 3 reports the luminescence lifetimes of the Re−xy$_n$−PhOH dyads and the reference complex in four different solvents (or solvent mixtures). In

dx.doi.org/10.1021/ja3053046 | J. Am. Chem. Soc. 2012, 134, 12844−12854

Table 3. Luminescence Lifetimes (τ) and Effective H/D Kinetic Isotope Effects (KIE_{eff}) for the Four Dyads from Scheme 1b and the $[Re(phen)(CO)_3(py)]^+$ Reference Complex in Various Solvents under Deoxygenated Conditions[a]

	τ (ns)				
	CH_2Cl_2	CH_3CN	CH_3CN/H_2O	CH_3CN/D_2O	KIE_{eff}
Re-ref	1220	1239	1270	1588	
Re−xy_0−PhOH	1141	986	40	95	2.0 ± 0.4
Re−xy_1−PhOH	970	582	144	194	1.1 ± 0.2
Re−xy_2−PhOH	902	1041	928	1254	
Re−xy_3−PhOH	1136	1151	1005	1378	

[a]Excitation occurred at 410 nm with 8 ns laser pulses, and detection was at 550 nm. See the text for definition of KIE_{eff}.

deoxygenated dichloromethane (second column), the lifetimes of the dyads do not differ significantly from that of the reference complex. In deoxygenated acetonitrile (third column), the lifetime of Re−xy_1−PhOH is markedly shorter than those of all the other systems, indicating that an additional nonradiative excited-state deactivation mechanism becomes competitive with ^{3}MLCT deactivation processes that are inherent to the $[Re(phen)(CO)_3(py)]^+$ complex. Triplet−triplet energy transfer has already been ruled out as a possible quenching source (see above), but photoinduced electron transfer is a viable possibility, particularly upon consideration of the ΔG_{ET} values in Table 2: ΔG_{ET} is negative for Re−xy_{1-3}−PhOH, but rate constants for electron tunneling (which we expect to be the relevant mechanism for CT in the specific cases of our molecules) decrease exponentially with increasing distance,[61,62,70] which may explain the absence of significant quenching for the Re−xy_n−PhOH dyads with n = 2 and n = 3 in CH_3CN. For the system with n = 0, there is no driving-force for photoinduced electron transfer (ΔG_{ET} = 0 eV) which may account for the absence of luminescence lifetime quenching in this dyad in pure CH_3CN. The transient absorption data presented below provide more direct evidence for photoinduced electron transfer in the Re−xy_1−PhOH dyad.

In a 1:1 (v/v) mixture of acetonitrile and water (Table 3, fourth column), we observed significant lifetime shortening for the Re−xy_n−PhOH dyads with n = 0−2, and only the longest member of the series appeared to exhibit emission that was essentially unquenched with respect to the reference complex. Thus, water is an essential ingredient for inducing substantial excited-state quenching in the Re−xy_n−PhOH dyads. Interestingly, somewhat longer lifetimes were measured when water was replaced by heavy water (fifth column); Figure 4 shows a direct comparison of luminescence lifetimes (τ) measured in CH_3CN/H_2O (faster decays of a given color) and CH_3CN/D_2O (slower decays of a given color). The largest H/D kinetic isotope effect (KIE) was detected for Re−xy_0−PhOH (τ_H/τ_D = 2.4) and the smallest for Re-ref (τ_H/τ_D = 1.3). The observation of a KIE for the reference complex most likely reflects the fact that multiphonon relaxation of the ^{3}MLCT excited state is less effective in the deuterated solvent, and this can be expected to occur in all three dyads. Thus, we find it useful to define an effective KIE (KIE_{eff}) in which this solvent effect on multiphonon relaxation has been factored out; KIE_{eff} therefore

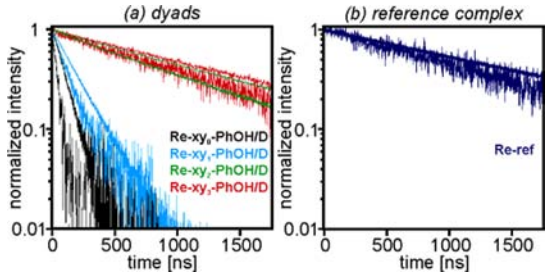

Figure 4. (a) Decays of the luminescence signals of the Re−xy_n−PhOH molecules in deoxygenated 1:1 (v/v) CH_3CN/H_2O (faster decays of a given color) and CH_3CN/D_2O (slower decays of a given color) after pulsed excitation at 410 nm (pulse width ∼8 ns); intensities have been arbitrarily normalized to a value of 1 at t = 0. (b) Luminescence decay of the reference complex under identical conditions.

reflects the true H/D KIE of the photochemistry occurring from ^{3}MLCT-excited rhenium(I). The resulting effective KIEs are reported in the last column of Table 3, and we note that only for the Re−xy_0−PhOH dyad does KIE_{eff} differ significantly from 1.0. The KIE_{eff} value obtained for the shortest dyad (2.0 ± 0.4) suggests that the rate-determining excited-state deactivation process involves proton motion, while in the longer dyads, most likely only electron motion involved. Since the luminescence quenching was rather weak in Re−xy_2−PhOH and Re−xy_3−PhOH, we have refrained from reporting KIEs for these two dyads (also see the comments below).

Equation 2 is commonly used to estimate rate constants for excited-state quenching (k_Q) from luminescence lifetimes:

$$k_Q = \tau^{-1} - \tau_{ref}^{-1} \quad (2)$$

where τ is the luminescence lifetime of the species of interest (here Re−xy_n−PhOH) and τ_{ref} is the luminescence lifetime of the reference species (Re-ref in the present case). Rate constants determined in this manner for CH_3CN/H_2O and CH_3CN/D_2O solutions of the Re−xy_n−PhOH molecules are displayed as functions of the donor−acceptor distance R_{DA} in the semilogarithmic plot of Figure 5. Data measured using CH_3CN/H_2O and CH_3CN/D_2O are shown in red and green, respectively. The heights of the vertical lines represent the error bars associated with the individual k_Q values and are based on the experience that each of the luminescence lifetimes could be determined with an experimental accuracy of ±10%. The error

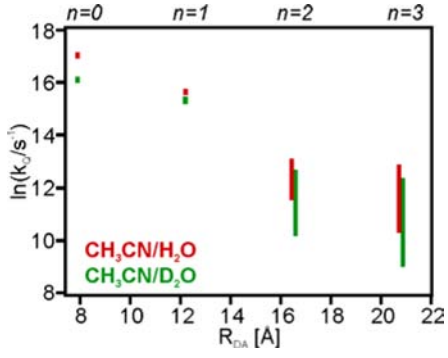

Figure 5. Semilogarthmic representation of the excited-state quenching rate constant k_Q as a function of the phenol−rhenium center-to-center distance R_{DA} in the four Re−xy_n−PhOH molecules in CH_3CN/H_2O (red) and CH_3CN/D_2O (green).

bars increase rapidly with increasing R_{DA} and get very large for Re−xy_2−PhOH and Re−xy_3−PhOH because the luminescence lifetimes of these two dyads approach that of the reference complex (Table 3).

Despite the large error bars, it is possible to discern a nearly exponential distance dependence of k_Q, as would be expected for intramolecular electron or hole tunneling across the *p*-xylene spacers. In view of the observation of KIE_{eff} values that differ significantly between Re−xy_0−PhOH and its longer congeners and upon consideration of the changeover in excited-state quenching mechanism that is most likely associated with this difference in KIE_{eff} (see above), it appears reasonable to extract a distance decay constant (the so-called β value) for k_Q from the data for Re−xy_n−PhOH with n = 1−3 and to exclude the dyad with n = 0 from this analysis; the transient absorption data shown below strongly support this procedure. From a linear regression fit to the CH_3CN/H_2O data in Figure 5, we thus found $\beta = 0.45 \pm 0.18$ Å^{-1}, while the CH_3CN/D_2O data yielded $\beta = 0.39 \pm 0.18$ Å^{-1}. These distance decay constants are in line with those found for analogous oligo-*p*-xylene and oligo-*p*-phenylene systems,[55,71] but it is to be noted that β is not a bridge-specific parameter but rather a function of the entire donor−bridge−acceptor construct.[61,62,72]

Transient Absorption Spectroscopy. Figure 6a shows transient absorption data obtained after excitation of the two

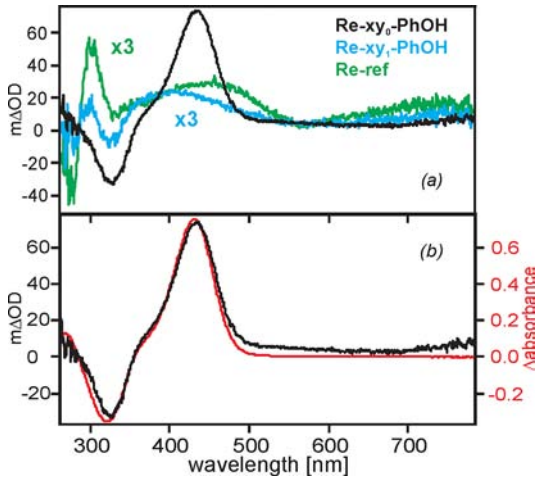

Figure 6. (a) Transient absorption spectra of Re−xy_n−PhOH (n = 0, 1) and Re-ref in deoxygenated 1:1 (v/v) acetonitrile/water. Excitation occurred at 355 nm with laser pulses having a width of ∼8 ns. Detection was in a time window of 200 ns after the laser pulse. (b) Superposition of the experimental transient absorption spectrum of Re−xy_0−PhOH (black trace) and a derived spectrum (red trace) obtained from subtraction of the absorption spectrum of Re−xy_0−PhOH at pH 7.9 (black trace in Figure 3a) from the absorption spectrum of Re−xy_0−PhOH at pH 12.4 (red trace in Figure 3a).

shortest dyads and the reference complex in deoxygenated 1:1 (v/v) CH_3CN/H_2O solutions at 355 nm with laser pulses having a width of ∼8 ns. The spectra were recorded by time averaging over the first 200 ns after the laser pulse. The reference complex exhibits a transient absorption spectrum that is typical for ^{3}MLCT-excited rhenium(I) tricarbonyl diimines (green trace): there is a bleach of the $\pi-\pi^*$ absorption of neutral phen at 275 nm along with a positive transient absorption signal at 300 nm characteristic of the reduced phen ligand.[73]. The signals decay with lifetimes of 1217 and 1324 ns, respectively, both in line with the luminescence lifetime measured for this compound under identical conditions (Table 3, fourth column).

The transient absorption spectrum of the Re−xy_1−PhOH dyad (blue trace) looks qualitatively similar to that of the reference complex, suggesting at first glance that one primarily observes the spectral signature of the ^{3}MLCT excited state in this case. A subtle but important difference relative to the spectrum of Re-ref (purple trace) is the occurrence of a relatively weak bleach at 325 nm, the wavelength at which the ground-state absorption spectrum of Re−xy_1−PhOH exhibits a shoulder that we attributed above to an electronic transition with phenol-to-pyridine CT character (Figure 2a). This particular bleach is diagnostic of the one-electron-reduced rhenium complex, and this fact will be important below in the discussion of the reaction kinetics of the Re−xy_1−PhOH dyad. Here we focus primarily on the transient absorption spectrum measured for the Re−xy_0−PhOH molecule (black trace in Figure 6a).

The transient absorption spectrum of the shortest dyad (black traces in Figure 6a,b) differs very significantly from those of the Re−xy_1−PhOH dyad and the reference complex. At comparable excitation pulse energies and dyad concentrations, not only are the observed changes in optical density (ΔOD) substantially higher (suggesting longer-lived photoproducts), but there are also significant spectral differences: the bleach at 275 nm and the positive signal at 300 nm (usually indicative of $phen^-$) are absent, but there is now a new bleach at 330 nm and a new absorption with a peak at 435 nm. The red trace in Figure 6b was obtained by subtracting the Re−xy_0−PhOH absorption spectrum at pH 7.9 (black trace in Figure 3a) from the respective absorption spectrum at pH 12.4 (red trace in Figure 3a). The superposition of this derived spectrum and the experimental transient absorption spectrum in Figure 6b demonstrates quite convincingly that photoexcitation of Re−xy_0−PhOH induces phenol deprotonation. In other words, the Re−xy_0−PhOH dyad acts as a photoacid. This finding is in line with the absence of luminescence lifetime quenching in this dyad in CH_2Cl_2 and pure CH_3CN (Table 3, second and third columns), where no protonatable reaction partners are available. In contrast, in acetonitrile/water mixtures, protonation of OH^- or H_2O species may occur, and excited-state quenching is comparatively rapid (Table 3, fourth and fifth columns). Furthermore, this finding is in line with the occurrence of a significant KIE for excited-state quenching in Re−xy_0−PhOH (KIE_{eff} = 2.0 ± 0.4; Table 3). Excited-state deactivation by proton transfer also makes sense in view of the fact that there is essentially no driving force for photoinduced electron transfer in this particular dyad (Table 2, last column).

Charge Transfer Kinetics in Re−xy_1−PhOH. In a prior section, we interpreted excited-state quenching in the three longer dyads (Re−xy_{1-3}−PhOH) in terms of photoinduced electron transfer because there is significant exergonicity associated with this process (contrary to Re−xy_0−PhOH) and because there is no significant H/D KIE in the luminescence quenching data (Table 3); moreover, triplet−triplet energy transfer quenching is thermodynamically unlikely. Unfortunately, the transient absorption spectrum of Re−xy_1−PhOH in Figure 6a (light-blue trace) failed to provide completely unambiguous evidence for oxidation products. Phenol radical cations and phenoxyl radicals have well-defined absorptions in the 350−500 nm spectral range,[74,75] but we were unable to detect any of these species unambiguously by transient absorption spectroscopy because in the same spectral

range there appear to be absorptions from the reduced rhenium moiety. The spectral signature of the reduced rhenium complex in turn is somewhat difficult to distinguish from the spectrum of ^{3}MLCT-excited rhenium because the dominant features are a bleach at 275 nm and a positive signal at 300 nm due to transient reduction of the phen ligand,[73,88] but this is the case not only for the one-electron-reduced form of the complex but also for its ^{3}MLCT-excited form. As mentioned above, the most diagnostic feature of the one-electron-reduced rhenium complex in Re−xy$_1$−PhOH is the weak bleach observed at 325 nm (blue trace in Figure 6a). This bleach cannot be observed for ^{3}MLCT-excited [Re(phen)(CO)$_3$(py)]$^+$.

Figure 7 shows the temporal evolution of the diagnostic bleach at 325 nm for Re−xy$_1$−PhOH in 1:1 (v/v) CH_3CN/H_2O (black trace) and 1:1 (v/v) CH_3CN/D_2O (red trace) after excitation at 355 nm with laser pulses of ∼8 ns duration. The two transients are noticeably different, both in the formation part of the bleach and in regard to the bleach recovery at times longer than 100−250 ns.

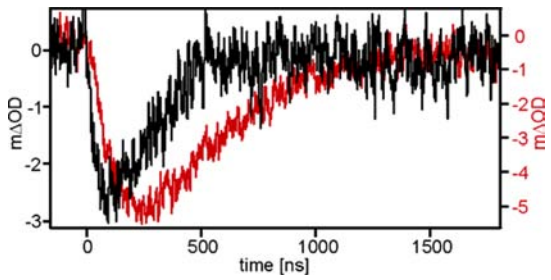

Figure 7. Temporal evolution of the transient absorption signals of Re−xy$_1$−PhOH at 325 nm in deoxygenated 1:1 (v/v) CH_3CN/H_2O (black trace) and 1:1 (v/v) CH_3CN/D_2O (red trace) after pulsed excitation at 355 nm. The pulse width was ∼8 ns.

We analyzed the two transients in Figure 7 using a kinetic model for an A → B → C reaction sequence. In this model, A is the initial photoexcited state, B is the charge-separated state with reduced rhenium, and C is the final (ground) state (Scheme 3a). From a fit to the black transient in Figure 7 we obtained time constants of 148 and 85 ns (Table 4). It appears tempting and most straightforward to associate the faster component (85 ns) to the buildup of state B (the A → B step), while the slower time constant (148 ns) would be attributed to the disappearance of state B (the B → C step). However, in A → B → C reaction sequences, the rise time for the population of state B need not necessarily correspond to the kinetics of the A → B reaction step but may instead reflect the kinetics of the B → C step.[54,76,77] There is evidence for exactly this scenario in the case of the Re−xy$_1$−PhOH dyad in CH_3CN/H_2O solution because the slower time constant (148 ns) in fact closely approaches the ^{3}MLCT lifetime extracted from luminescence measurements (144 ns; Table 3). In the luminescence experiments, we monitored the disappearance of state A (the A → B step), and hence it appears plausible to conclude that the 148 ns component in the transient absorption data is in fact due to the A → B step. In this picture, the 85 ns time constant is then due to the B → C step.

From a similar analysis of the red transient in Figure 7 (i.e., the data obtained for the same dyad in CH_3CN/D_2O), we obtained time constants of 169 and 313 ns (Table 4). The ^{3}MLCT lifetime extracted from luminescence measurements in this case was 194 ns (Table 3), so it appears plausible to assign the 169 ns time constant observed in transient absorption spectroscopy to the A → B step, while the 313 ns time constant then logically would be due to the B → C reaction step. In view of the fact that we have two complementary sets of data (time-resolved luminescence and transient absorption), these assignments appear plausible.[78]

In the framework of our kinetic model, the B → C reaction step is associated with a sizable H/D KIE of 3.7 ± 0.5 (i.e., the ratio of 313 and 85 ns), which cannot be reconciled with simple electron transfer. Indeed, this H/D KIE strongly suggests that there is proton movement in the B → C reaction step. This appears peculiar at first glance, but we think there is a very plausible explanation for this observation (Scheme 3b): once intramolecular phenol-to-rhenium(I) electron transfer has occurred, the oxidized phenol radical cation is a highly acidic species; in the case of tyrosine, the pK_a of the phenolic proton drops from a value of ∼9 in the charge-neutral form to a value of around −2 in the oxidized species.[17,33,79] It therefore appears plausible to assume that when water is present (pK_a for H_3O^+ = −1.7), the oxidized phenol releases a proton, forming a neutral phenoxyl radical. This hypothesis is illustrated by Scheme 3b, which gives a more accurate description of the photoinduced chemistry in Re−xy$_1$−PhOH than Scheme 3a: after the rate-determining initial electron transfer step forming "state B$_1$" (with oxidized but still protonated phenol), there is rapid proton release to H_2O, thereby forming "state B$_2$" (with reduced rhenium, neutral phenoxyl radical, and protonated water); however, in time-resolved luminescence and transient absorption, we monitor only the A → B$_1$ step, but re-establishment of the original rhenium(I) dyad (state C) via intramolecular electron transfer must be coupled to reprotonation of the phenol moiety. This may explain the occurrence of the significant KIE in the B$_2$ → C step (observable in transient absorption spectroscopy).[80]

Charge Transfer Kinetics in Re−xy$_0$−PhOH. We now turn our attention back to the transient absorption data obtained from the Re−xy$_0$−PhOH dyad. On the basis of the data in Figure 6b, we concluded above that this molecule acts

Scheme 3. Reaction Sequence Models for Re−xy$_1$−PhOH

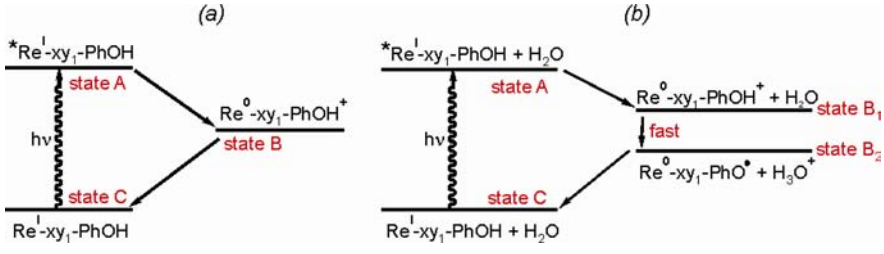

dx.doi.org/10.1021/ja3053046 | J. Am. Chem. Soc. 2012, 134, 12844−12854

Table 4. Transient Absorption Lifetimes and H/D Kinetic Isotope Effects for Excited-State Quenching and Charge Recombination in Re−xy$_0$−PhOH and Re−xy$_1$−PhOH in Deoxygenated 1:1 (v/v) CH_3CN/H_2O and CH_3CN/D_2O[a]

	excited-state quenching			thermal charge recombination		
	τ_H (ns)	τ_D (ns)	KIE_{eff}	τ_H (ns)	τ_D (ns)	KIE
Re−xy$_0$−PhOH	43[b]/41[c]/36[d]	95[b]/86[c]/76[d]	1.8 ± 0.3[b,c,d]	13200[c]/14000[d]	47200[c]/49200[d]	3.6 ± 0.5[c]/3.5 ± 0.5[d]
Re−xy$_1$−PhOH	148[c]	169[c]	1.0 ± 0.3[c]	85[c]	313[c]	3.7 ± 0.5[c]

[a]Excitation occurred at 355 nm with 8 ns laser pulses. τ_H = lifetime in CH_3CN/H_2O; τ_D = lifetime in CH_3CN/D_2O. [b]Detected at 275 nm. [c]Detected at 325 or 330 nm. [d]Detected at 435 nm.

essentially as a photoacid, but we have not yet presented and discussed the reaction kinetics of this dyad.

Figure 8a shows the temporal evolution of the phenol-based transient absorption signals of Re−xy$_0$−PhOH at 435 nm (upper half) and 330 nm (lower half). The black traces were measured in deoxygenated 1:1 (v/v) CH_3CN/H_2O and the red traces in deoxygenated 1:1 (v/v) CH_3CN/D_2O. It is obvious from these data that there is a significant H/D KIE. The specific rise times of these signals are on the order of 40 ns for protonated samples (Table 4, second column) and on the order of 80 ns for deuterated samples (Table 4, third column), yielding a KIE of 1.8 ± 0.3. These transient absorption data are fully consistent with the findings from time-resolved luminescence spectroscopy (Table 3).

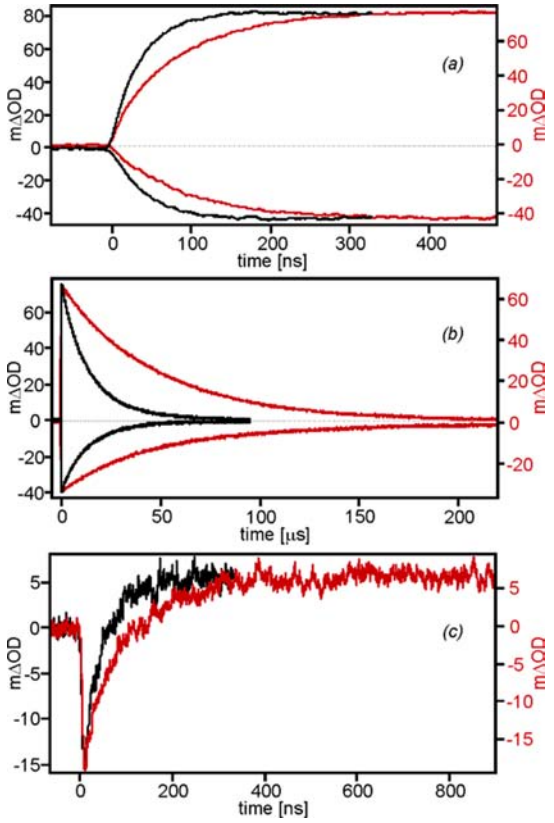

Figure 8. Temporal evolution of the transient absorption signals of Re−xy$_0$−PhOH in deoxygenated 1:1 (v/v) CH_3CN/H_2O (black traces) and 1:1 (v/v) CH_3CN/D_2O (red traces) at various detection wavelengths: (a, b) 435 nm (upper traces) and 330 nm (lower traces); (c) 275 nm. The different time scales in (a) and (b) should be noted. Excitation occurred with 8 ns laser pulses at 355 nm in all cases.

Figure 8c shows the temporal evolution of the transient absorption signal of Re−xy$_0$−PhOH at 275 nm (the bleach of neutral phen). The black traces were measured in 1:1 (v/v) CH_3CN/H_2O and the red traces in 1:1 (v/v) CH_3CN/D_2O. The time constants for the recovery of these bleaches are 43 and 95 ns for the protonated and deuterated species, respectively (Table 4), giving a H/D KIE similar to that found above from the time-resolved luminescence experiments (Table 3). This finding is consistent with release of the phenolic proton by the photoexcited Re−xy$_0$−PhOH to the bulk solvent coupled with simultaneous relaxation to the electronic ground state.

Figure 8b shows the decays of the transient absorption signals of Re−xy$_0$−PhOH at 435 nm (upper half) and 330 nm (lower half). The decays are remarkably slow and occur with time constants of 14.0 and 13.2 μs, respectively, in CH_3CN/H_2O, and 49.2 and 47.2 μs, respectively, in CH_3CN/D_2O. Thus, as in the case of the longer Re−xy$_1$−PhOH dyad, the rate-determining step leading the photoproducts back to the initially present species is associated with a significant H/D KIE. In the specific case of the Re−xy$_0$−PhOH dyad, we found KIEs of 3.5 ± 0.5 (435 nm) and 3.6 ± 0.5 (330 nm), while for Re−xy$_1$−PhOH, we found a KIE of 3.7 ± 0.5 (Table 4, last column).

The observation of photoproducts with microsecond lifetimes after photoexcitation of Re−xy$_0$−PhOH is interesting, particularly in view of the fact that the Re−xy$_1$−PhOH photoproducts exhibit lifetimes on the order of only ∼100 ns (Table 3). We think this discrepancy mainly stems from the fact that the photoproducts are different in these two dyads: the shorter molecule reacts to give a Re(I)−xy$_0$−PhO$^-$ species with a phenolate anion (at least formally; see the comments below), while the longer congener gives a Re(0)−xy$_1$−PhO$^\bullet$ species with a phenoxyl radical (the B_2 state in Scheme 3b). The driving forces and reorganization energies for re-establishing the initial Re(I)−xy$_0$−PhOH and Re(I)−xy$_1$−PhOH species would be expected to be significantly different, and this could easily be manifested in substantially different reaction kinetics. In addition, we note that for the Re(I)−xy$_0$−PhO$^-$ species, the resonance structure on the right-hand side of Scheme 2 is presumably more important. Furthermore, it appears plausible to state that this resonance structure would be less easily reprotonated at the oxygen atom than the phenolate structure on the left-hand side of Scheme 2.

Transient absorption experiments with the longer Re−xy$_2$−PhOH and Re−xy$_3$−PhOH dyads were largely inconclusive because the photoinduced chemistry in these systems is too slow with respect to the inherent ^{3}MLCT lifetime of the rhenium(I) photosensitizer. Hence, the time-resolved absorption studies were limited to the two shortest dyads.

Possible Reasons for Different Photoreactivities of Re−xy$_0$−PhOH and Re−xy$_1$−PhOH. In the Cyclic Voltammetry section, we noted that the phenol oxidations and some of the rhenium (or more precisely the phenanthroline-based) reductions in our dyads are irreversible in cyclic voltammetry. Thus, there is significant uncertainty in the redox potential

dx.doi.org/10.1021/ja3053046 | J. Am. Chem. Soc. 2012, 134, 12844−12854

values reported in Table 2. Nevertheless, it seems clear that the Re–xy_0–PhOH molecule stands out from the dyad series in that it has a phenol oxidation potential which is ~0.2 V more positive than in the longer dyads. Use of eq 1 has led us to the conclusion that photoinduced electron transfer from the phenol units to photoexcited rhenium(I) complexes should be slightly exergonic in the Re–xy_{1-3}–PhOH dyads ($\Delta G_{ET} \approx -0.2$ eV; Table 2, last column), whereas we expect essentially no driving force in Re–xy_0–PhOH. We think that this is one of the key reasons for the different photoreactivities of the Re–xy_0–PhOH and Re–xy_1–PhOH dyads. Another important reason may be the possible resonance stabilization of the phenolate anion in Re–xy_0–PhOH; the fact that the phenolate–pyridine unit may adopt a stable quinonoid structure (right half of Scheme 2)[81] may potentially provide a significant driving force for phototriggered proton release. Scheme 4 illustrates the situation in Re–xy_0–PhOH. Initial photoexcitation populates mainly the emissive ^{3}MLCT state, which is energetically below the phenol → pyridine CT state. Upon deprotonation (possibly involving the phenol → pyridine CT state itself), the phenol → pyridine CT state is energetically stabilized because it is now a *phenolate* → pyridine CT state. This leads to emission quenching and provides the driving force for the transfer of electron density from the phenolate unit toward the metal center.

Scheme 4. Energy-Level Scheme Showing the Most Relevant Excited States of Re–xy_0–PhOH (a) before and (b) after Deprotonation

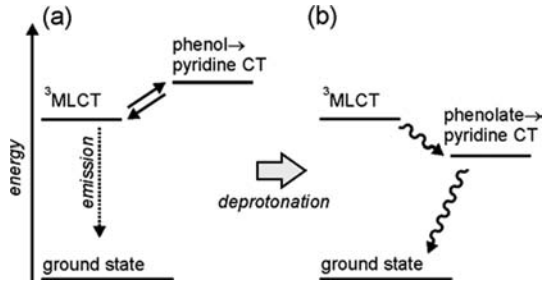

In the Re–xy_1–PhOH dyad, we expect the phenomenon of different resonance structures to play a much less important role because the phenol and pyridine units are electronically decoupled from each other by an intervening *p*-xylene spacer.

SUMMARY AND CONCLUSIONS

The initial aim of this work was to explore how variation of the distance between the electron-accepting and electron/proton-donating sites affects the rates and mechanism of bidirectional (multisite) PCET in rhenium–(oligo-*p*-xylene)–phenol molecules. We anticipated that all four dyads shown in Scheme 1b would exhibit photoinduced PCET chemistry in acetonitrile/water mixtures and wondered how the PCET rates and mechanisms would change with increasing phenol–rhenium distance. Interestingly, we found that the Re–xy_0–PhOH dyad acts as a photoacid, while the Re–xy_1–PhOH molecule exhibits photoinduced PCET chemistry involving a stepwise ETPT reaction sequence. However, to some extent, the term "photoacid" does not sufficiently accurately describe the photoinduced chemistry of the Re–xy_0–PhOH dyad because the deprotonated phenol–pyridine ligand has two resonance structures (Scheme 2). When considering the quinonoid structure at the right in Scheme 2, one may note that electron transfer from the phenolate moiety to the pyridine moiety has taken place; with some caution, one may therefore consider the overall photoreaction of Re–xy_0–PhOH in acetonitrile/water as a variant of PCET. At any rate, it is clear from our transient absorption studies that the rate-determining steps in the photoinduced reactions of the donor–acceptor molecule Re–xy_0–PhOH and the donor–bridge–acceptor compound Re–xy_1–PhOH are different: proton motion is involved in the case of the shortest dyad (KIE = 1.8 ± 0.3), while in Re–xy_1–PhOH there is no significant KIE for the photoinduced forward reaction (as determined by the combination of time-resolved emission and transient absorption studies). In contrast, the thermal backward reaction of Re–xy_1–PhOH (like that of Re–xy_0–PhOH) exhibits a H/D KIE of >3, indicating that proton motion is important in the rate-determining step leading back to the initially present species. Thus, our study provides significant new insight into photoinduced PCET chemistry, particularly with respect to the influence of the donor–acceptor distance on the overall reaction and the importance of strong electronic coupling between the donor and acceptor units.

EXPERIMENTAL SECTION

Synthesis, Electrochemistry, and Optical Spectroscopy. Detailed synthetic protocols and characterization data for the four dyads from Scheme 1b are given in the Supporting Information. Thin-layer chromatography was performed using Polygram SIL G/UV254 plates from Machery-Nagel, and for column chromatography, Silica Gel 60 from the same company was employed. Reaction products were characterized by ^{1}H spectroscopy on a Bruker Avance DRX 300 spectrometer, by electrospray ionization mass spectrometry using a Bruker APEX IV (FTICR-MS) instrument, and by elemental analysis (conducted by Susanne Petrich at the Institute for Inorganic Chemistry, Göttingen). Optical absorption spectroscopy was performed using Cary 50 and Cary 300 spectrophotometers from Varian, and steady-state luminescence spectra were measured on a Fluorolog-3 instrument (FL322) from HORIBA Jobin Yvon. For time-resolved luminescence and transient absorption spectroscopy, an LP920-KS instrument from Edinburgh Instruments, equipped with a Hamamatsu photomultiplier and an iCCD camera from Andor, was used. The excitation source was a Quantel Brilliant b laser equipped with an optical parametric oscillator from Opotek. A VersaSTAT 3-200 potentiostat from Princeton Applied Research was used for cyclic voltammetry. A glassy carbon electrode served as the working electrode, and two silver wires were used as counter and quasi-reference electrodes. Ferrocene was used as an internal reference. Prior to voltage scans at rates of 100 mV/s, nitrogen gas was bubbled through the dried solvent. The supporting electrolyte was a 0.1 M solution of $TBAPF_6$.

Crystal Structure Determination. The single crystal was mounted in inert oil under cryogenic conditions employing the X-Temp2 device.[82−84] The X-ray data set was collected at 100(2) K on an INCOATEC microfocus source[85] with mirror-monochromatized Mo Kα radiation (λ = 0.71073 Å) and equipped with a Bruker Smart Apex II detector and integrated with SAINT, and an empirical absorption correction with SADABS was applied.[86] The structure was solved with direct methods (SHELXS in SHELXTL, version 2008/3) and refined by full-matrix least-squares methods against F^2 (SHELXS in SHELXTL, version 2008/3).[87] All non-hydrogen atoms were refined with anisotropic displacement parameters. The hydrogen atoms were refined isotropically on calculated positions using a riding model with their U_{iso} values constrained to equal to 1.5 times the U_{eq} of their pivot atoms for terminal sp^3 carbon atoms and 1.2U_{eq} for all other carbon atoms. An exception was the O1 bonded H100, whose position was taken from the residual density map and refined freely.

In the crystal structure of Re–xy_1–PhOH, the diethyl ether solvent molecule was disordered at two positions. The molecule was set on a

special position, thus revealing a total of four positions. Disordered moieties were refined using bond length and displacement parameter restraints. Crystallographic data (excluding structure factors) for the structures reported in this paper have been deposited with the Cambridge Crystallographic Data Centre (CCDC) as supplementary publication no. 838939. Copies of the data can be obtained free of charge upon application to the CCDC, 12 Union Road, Cambridge CB2 1EZ, U.K. [fax, (internat.) +44(1223)336-033; e-mail, deposit@ccdc.cam.ac.uk].

■ ASSOCIATED CONTENT

Supporting Information

Detailed synthetic protocols and characterization data, additional electrochemical data, and crystallographic data for Re–xy_1–PhOH (CIF). This material is available free of charge via the Internet at http://pubs.acs.org.

■ AUTHOR INFORMATION

Corresponding Author

oliver.wenger@chemie.uni-goettingen.de

Notes

The authors declare no competing financial interest.

■ ACKNOWLEDGMENTS

This work was supported by the Deutsche Forschungsgemeinschaft (DFG) through IRTG 1422. The MWK Niedersachsen and the DFG (INST186/872-1) are thanked for funding the transient absorption setup. We kindly acknowledge funding from the DNRF-funded Centre of Materials Crystallography and the doctoral programme Catalysis for Sustainable Synthesis, provided by the Land Niedersachsen.

■ REFERENCES

(1) Mayer, J. M. *Annu. Rev. Phys. Chem.* **2004**, *55*, 363–390.
(2) Huynh, M. H. V.; Meyer, T. J. *Chem. Rev.* **2007**, *107*, 5004–5064.
(3) Reece, S. Y.; Nocera, D. G. *Annu. Rev. Biochem.* **2009**, *78*, 673–699.
(4) Magnuson, A.; Anderlund, M.; Johansson, O.; Lindblad, P.; Lomoth, R.; Polivka, T.; Ott, S.; Stensjö, K.; Styring, S.; Sundström, V.; Hammarström, L. *Acc. Chem. Res.* **2009**, *42*, 1899–1909.
(5) Hammes-Schiffer, S. *Acc. Chem. Res.* **2009**, *42*, 1881–1889.
(6) Dempsey, J. L.; Winkler, J. R.; Gray, H. B. *Chem. Rev.* **2010**, *110*, 7024–7039.
(7) Costentin, C.; Robert, M.; Savéant, J.-M. *Acc. Chem. Res.* **2010**, *43*, 1019–1029.
(8) Gagliardi, C. J.; Westlake, B. C.; Kent, C. A.; Paul, J. J.; Papanikolas, J. M.; Meyer, T. J. *Coord. Chem. Rev.* **2010**, *254*, 2459–2471.
(9) Cukier, R. I.; Nocera, D. G. *Annu. Rev. Phys. Chem.* **1998**, *49*, 337–369.
(10) Bordwell, F. G.; Cheng, J. P. *J. Am. Chem. Soc.* **1991**, *113*, 1736–1743.
(11) Warren, J. J.; Tronic, T. A.; Mayer, J. M. *Chem. Rev.* **2010**, *110*, 6961–7001.
(12) Biczok, L.; Gupta, N.; Linschitz, H. *J. Am. Chem. Soc.* **1997**, *119*, 12601–12609.
(13) Concepcion, J. J.; Brennaman, M. K.; Deyton, J. R.; Lebedeva, N. V.; Forbes, M. D. E.; Papanikolas, J. M.; Meyer, T. J. *J. Am. Chem. Soc.* **2007**, *129*, 6968–6969.
(14) Bronner, C.; Wenger, O. S. *J. Phys. Chem. Lett.* **2012**, *3*, 70–74.
(15) Mayer, J. M.; Rhile, I. J.; Larsen, F. B.; Mader, E. A.; Markle, T. F.; DiPasquale, A. G. *Photosynth. Res.* **2006**, *87*, 3–20.
(16) Lachaud, T.; Quaranta, A.; Pellegrin, Y.; Dorlet, P.; Charlot, M. F.; Un, S.; Leibl, W.; Aukauloo, A. *Angew. Chem., Int. Ed.* **2005**, *44*, 1536–1540.
(17) Magnuson, A.; Berglund, H.; Korall, P.; Hammarström, L.; Åkermark, B.; Styring, S.; Sun, L. C. *J. Am. Chem. Soc.* **1997**, *119*, 10720–10725.
(18) Sun, L. C.; Burkitt, M.; Tamm, M.; Raymond, M. K.; Abrahamsson, M.; LeGourriérec, D.; Frapart, Y.; Magnuson, A.; Kenéz, P. H.; Brandt, P.; Tran, A.; Hammarström, L.; Styring, S.; Åkermark, B. *J. Am. Chem. Soc.* **1999**, *121*, 6834–6842.
(19) Johansson, O.; Wolpher, H.; Borgström, M.; Hammarström, L.; Bergquist, J.; Sun, L. C.; Åkermark, B. *Chem. Commun.* **2004**, 194–195.
(20) Maki, T.; Araki, Y.; Ishida, Y.; Onomura, O.; Matsumura, Y. *J. Am. Chem. Soc.* **2001**, *123*, 3371–3372.
(21) Benisvy, L.; Bittl, R.; Bothe, E.; Garner, C. D.; McMaster, J.; Ross, S.; Teutloff, C.; Neese, F. *Angew. Chem., Int. Ed.* **2005**, *44*, 5314–5317.
(22) Rhile, I. J.; Markle, T. F.; Nagao, H.; DiPasquale, A. G.; Lam, O. P.; Lockwood, M. A.; Rotter, K.; Mayer, J. M. *J. Am. Chem. Soc.* **2006**, *128*, 6075–6088.
(23) Quaranta, A.; Lachaud, F.; Herrero, C.; Guillot, R.; Charlot, M. F.; Leibl, W.; Aukauloo, A. *Chem.—Eur. J.* **2007**, *13*, 8201–8211.
(24) Markle, T. F.; Rhile, I. J.; DiPasquale, A. G.; Mayer, J. M. *Proc. Natl. Acad. Sci. U.S.A.* **2008**, *105*, 8185–8190.
(25) Markle, T. F.; Mayer, J. M. *Angew. Chem., Int. Ed.* **2008**, *47*, 738–740.
(26) Moore, G. F.; Hambourger, M.; Gervaldo, M.; Poluektov, O. G.; Rajh, T.; Gust, D.; Moore, T. A.; Moore, A. L. *J. Am. Chem. Soc.* **2008**, *130*, 10466–10467.
(27) Rhile, I. J.; Mayer, J. M. *J. Am. Chem. Soc.* **2004**, *126*, 12718–12719.
(28) Costentin, C.; Robert, M.; Savéant, J.-M. *J. Am. Chem. Soc.* **2006**, *128*, 4552–4553.
(29) Reece, S. Y.; Nocera, D. G. *J. Am. Chem. Soc.* **2005**, *127*, 9448–9458.
(30) Bertini, I.; Gray, H. B.; Stiefel, E. I.; Valentine, J. S. *Biological Inorganic Chemistry*; University Science Books: Sausalito, CA, 2007.
(31) Sjödin, M.; Irebo, T.; Utas, J. E.; Lind, J.; Merenyi, G.; Åkermark, B.; Hammarström, L. *J. Am. Chem. Soc.* **2006**, *128*, 13076–13083.
(32) Sjödin, M.; Ghanem, R.; Polivka, T.; Pan, J.; Styring, S.; Sun, L. C.; Sundström, V.; Hammarström, L. *Phys. Chem. Chem. Phys.* **2004**, *6*, 4851–4858.
(33) Sjödin, M.; Styring, S.; Wolpher, H.; Xu, Y. H.; Sun, L. C.; Hammarström, L. *J. Am. Chem. Soc.* **2005**, *127*, 3855–3863.
(34) Irebo, T.; Johansson, O.; Hammarström, L. *J. Am. Chem. Soc.* **2008**, *130*, 9194–9195.
(35) Irebo, T.; Reece, S. Y.; Sjödin, M.; Nocera, D. G.; Hammarström, L. *J. Am. Chem. Soc.* **2007**, *129*, 15462–15464.
(36) Bonin, J.; Costentin, C.; Louault, C.; Robert, M.; Savéant, J.-M. *J. Am. Chem. Soc.* **2011**, *133*, 6668–6674.
(37) Bonin, J.; Costentin, C.; Louault, C.; Robert, M.; Routier, M.; Savéant, J.-M. *Proc. Natl. Acad. Sci. U.S.A.* **2010**, *107*, 3367–3372.
(38) Costentin, C.; Robert, M.; Savéant, J.-M. *J. Am. Chem. Soc.* **2007**, *129*, 5870–5879.
(39) Hankache, J.; Hanss, D.; Wenger, O. S. *J. Phys. Chem. A* **2012**, *116*, 3347–3358.
(40) Oevering, H.; Paddon-Row, M. N.; Heppener, M.; Oliver, A. M.; Cotsaris, E.; Verhoeven, J. W.; Hush, N. S. *J. Am. Chem. Soc.* **1987**, *109*, 3258–3269.
(41) Gray, H. B.; Winkler, J. R. *Proc. Natl. Acad. Sci. U.S.A.* **2005**, *102*, 3534–3539.
(42) Manner, V. W.; DiPasquale, A. G.; Mayer, J. M. *J. Am. Chem. Soc.* **2008**, *130*, 7210–7211.
(43) Manner, V. W.; Mayer, J. M. *J. Am. Chem. Soc.* **2009**, *131*, 9874–9875.
(44) Markle, T. F.; Rhile, I. J.; Mayer, J. M. *J. Am. Chem. Soc.* **2011**, *133*, 17341–17352.
(45) Zhang, M.-T.; Irebo, T.; Johansson, O.; Hammarström, L. *J. Am. Chem. Soc.* **2011**, *133*, 13224–13227.
(46) Walther, M. E.; Wenger, O. S. *Dalton Trans.* **2008**, 6311–6318.

(47) Hanss, D.; Walther, M. E.; Wenger, O. S. *Coord. Chem. Rev.* **2010**, *254*, 2584−2592.
(48) Hanss, D.; Wenger, O. S. *Inorg. Chem.* **2008**, *47*, 9081−9084.
(49) Hanss, D.; Wenger, O. S. *Inorg. Chem.* **2009**, *48*, 671−680.
(50) Walther, M. E.; Wenger, O. S. *ChemPhysChem* **2009**, *10*, 1203−1206.
(51) Bouzakraoui, S.; Bouzzine, S. M.; Bouachrine, M.; Hamidi, M. *J. Mol. Struct.* **2005**, *725*, 39−44.
(52) Lukeš, V.; Aquino, A. J. A.; Lischka, H.; Kauffmann, H. F. *J. Phys. Chem. B* **2007**, *111*, 7954−7962.
(53) Grave, C.; Risko, C.; Shaporenko, A.; Wang, Y. L.; Nuckolls, C.; Ratner, M. A.; Rampi, M. A.; Zharnikov, M. *Adv. Funct. Mater.* **2007**, *17*, 3816−3828.
(54) Hanss, D.; Wenger, O. S. *Eur. J. Inorg. Chem.* **2009**, 3778−3790.
(55) Weiss, E. A.; Ahrens, M. J.; Sinks, L. E.; Gusev, A. V.; Ratner, M. A.; Wasielewski, M. R. *J. Am. Chem. Soc.* **2004**, *126*, 5577−5584.
(56) Weiss, E. A.; Tauber, M. J.; Kelley, R. F.; Ahrens, M. J.; Ratner, M. A.; Wasielewski, M. R. *J. Am. Chem. Soc.* **2005**, *127*, 11842−11850.
(57) Hanss, D.; Walther, M. E.; Wenger, O. S. *Coord. Chem. Rev.* **2010**, *254*, 2584−2592.
(58) Sacksteder, L.; Zipp, A. P.; Brown, E. A.; Streich, J.; Demas, J. N.; DeGraff, B. A. *Inorg. Chem.* **1990**, *29*, 4335−4340.
(59) Wallace, L.; Rillema, D. P. *Inorg. Chem.* **1993**, *32*, 3836−3843.
(60) Cargill Thompson, A. M. W.; Smailes, M. C. C.; Jeffery, J. C.; Ward, M. D. *J. Chem. Soc., Dalton Trans.* **1997**, 737−743.
(61) Wenger, O. S. *Acc. Chem. Res.* **2011**, *44*, 25−35.
(62) Albinsson, B.; Eng, M. P.; Pettersson, K.; Winters, M. U. *Phys. Chem. Chem. Phys.* **2007**, *9*, 5847−5864.
(63) Connick, W. B.; Di Bilio, A. J.; Hill, M. G.; Winkler, J. R.; Gray, H. B. *Inorg. Chim. Acta* **1995**, *240*, 169−173.
(64) Das, P. K.; Encinas, M. V.; Scaiano, J. C. *J. Am. Chem. Soc.* **1981**, *103*, 4154−4162.
(65) Lafolet, F.; Welter, S.; Popovic, Z.; De Cola, L. *J. Mater. Chem.* **2005**, *15*, 2820−2828.
(66) Hevia, E.; Perez, J.; Riera, L.; Riera, V.; del Rio, I.; Garcia-Granda, S.; Miguel, D. *Chem.—Eur. J.* **2002**, *8*, 4510−4521.
(67) Weller, A. *Z. Phys. Chem.* **1982**, *133*, 93−98.
(68) Gagliardi, L. G.; Castells, C. B.; Rafols, C.; Roses, M.; Bosch, E. *J. Chem. Eng. Data* **2007**, *52*, 1103−1107.
(69) Gagliardi, L. G.; Castells, C. B.; Rafols, C.; Roses, M.; Bosch, E. *Anal. Chem.* **2007**, *79*, 3180−3187.
(70) McConnell, H. M. *J. Chem. Phys.* **1961**, *35*, 508−515.
(71) Wenger, O. S. *Chem. Soc. Rev.* **2011**, *40*, 3538−3550.
(72) Eng, M. P.; Albinsson, B. *Angew. Chem., Int. Ed.* **2006**, *45*, 5626−5629.
(73) Chen, P. Y.; Westmoreland, T. D.; Danielson, E.; Schanze, K. S.; Anthon, D.; Neveux, P. E.; Meyer, T. J. *Inorg. Chem.* **1987**, *26*, 1116−1126.
(74) Das, P. K.; Encinas, M. V.; Steenken, S.; Scaiano, J. C. *J. Am. Chem. Soc.* **1981**, *103*, 4162−4166.
(75) Gadosy, T. A.; Shukla, D.; Johnston, L. J. *J. Phys. Chem. A* **1999**, *103*, 8834−8839.
(76) Atkins, P. W.; de Paula, J. *Physical Chemistry*, 8th ed.; Oxford University Press: Oxford, U.K., 2006.
(77) Borgström, M.; Johansson, O.; Lomoth, R.; Baudin, H. B.; Wallin, S.; Sun, L. C.; Åkermark, B.; Hammarström, L. *Inorg. Chem.* **2003**, *42*, 5173−5184.
(78) Transient IR spectroscopy might be able to provide additional insight, but this experimental method is not readily available.
(79) Sjödin, M.; Styring, S.; Åkermark, B.; Sun, L. C.; Hammarström, L. *J. Am. Chem. Soc.* **2000**, *122*, 3932−3936.
(80) Our transient absorption experiments monitor the reappearance of state C.
(81) Alternatively, the relevant structure might be called a pyridone-like structure.
(82) Kottke, T.; Stalke, D. *J. Appl. Crystallogr.* **1993**, *26*, 615−619.
(83) Kottke, T.; Lagow, R. J.; Stalke, D. *J. Appl. Crystallogr.* **1996**, *29*, 465−468.
(84) Stalke, D. *Chem. Soc. Rev.* **1998**, *27*, 171−178.
(85) Schulz, T.; Meindl, K.; Leusser, D.; Stern, D.; Graf, J.; Michaelsen, C.; Ruf, M.; Sheldrick, G. M.; Stalke, D. *J. Appl. Crystallogr.* **2009**, *42*, 885−891.
(86) Sheldrick, G. M. *SADABS 2008/2*; University of Göttingen: Göttingen, Germany, 2008.
(87) Sheldrick, G. M. *Acta Crystallogr., Sect. A.* **2008**, *64*, 112−122.
(88) Záliš, S.; Cosani, C.; Cannizzo, A.; Chergui, M.; Hartl, F.; Vlček, A., Jr. *Inorg. Chim. Acta* **2011**, *374*, 578−585.